

The age-mass relation for chromospherically active binaries

III. Lithium depletion in giant components^{*}

D. Barrado y Navascués^{1,2}, E. De Castro³, M.J. Fernández-Figueroa³, M. Cornide³, and R.J. García López⁴

¹ MEC/Fulbright Fellow at the Smithsonian Astrophysical Observatory, 60 Garden St, Cambridge, MA 02138, USA.

² Real Colegio Complutense at Harvard University, Trowbridge St, Cambridge, MA 02138, USA.

³ Dpto. Astrofísica. Facultad de Físicas. Universidad Complutense. E-28040 Madrid, Spain.

⁴ Instituto de Astrofísica de Canarias. E-38200 La Laguna, Tenerife, Spain.

Received date, ; accepted date,

Abstract. We present a study of the lithium abundances of a sample of evolved components of Chromospherically Active Binary Systems. We show that a significant part of them have lithium excesses, independently of their mass and evolutionary stage. Therefore, it can be concluded that Li abundance does not depend on age for giant components of CABS. These overabundances appear to be closely related to the stellar rotation, and we interpret them as a consequence of the transfer of angular momentum from the orbit to the rotation as the stars evolve in and off the Main Sequence, in a similar way as it happens in the dwarf components of the same systems and in the Tidally Locked Binaries belonging to the Hyades and M67.

Key words: stars: abundances – stars: activity – stars: binaries: close – stars: late-type – stars: rotation – stars: evolution

1. Introduction

This is the third paper of a series devoted to the study of the stellar properties of Chromospheric Active Binary Systems (CABS). This heterogeneous group of stars includes systems which have evolved components together with binaries with both members inside the Main Sequence (MS). Strassmeier et al. (1993) presented a characterization of

this type of binaries and a catalog complete up to that date. In Paper I (Barrado et al. 1994), we studied the evolutionary status of CABS using the effective temperature (T_{eff})–Radii plane and estimated their ages by comparing masses, radii and temperatures for both components with theoretical isochrones. The main conclusion of that paper is that CABS are in a particular stage of their stellar evolution. The high stellar activity appears in CABS when one of the components is evolving off (or has already done so) the MS, crossing the Terminal Age Main Sequence (TAMS). Classifying the systems on the T_{eff} –Radii plane, we established in Paper I that CABS appear divided in three different groups: MS stars with masses $<1.7 M_{\odot}$, evolved stars with masses close to $1.4 M_{\odot}$, and giant stars having masses in the interval $2.5\text{--}5.0 M_{\odot}$. The second group could be subdivided into other three types: subgiants evolving off the MS, subgiants at the bottom of the Red Giant Branch (RGB), and giants ascending the RGB above the previous sub-classification. However, not all CABS have accurate values of radii and masses making so impossible their location in any of these groups using these criteria. For this reason, Paper II (Barrado y Navascués et al. 1997) used other strategy to classify the components of CABS. We studied the evolutionary status of the whole sample of CABS listed in Strassmeier et al. (1993) using the photometry. Visual magnitudes, colors, and individual distances (when available), allowed us to locate the stars in a Color–Magnitude Diagram (CMD). CABS are concentrated in specific regions: MS stars, stars evolving off the MS, those at the bottom and at the top part of the RGB (B–RGB and T–RGB, respectively) and components located in what we called the horizontal branch (HB) due to its geometrical configuration. Note that our nomenclature does not refer to the real horizontal branch, formed by RR Lyrae and other types of stars. The CABS have masses around $5 M_{\odot}$ and are first

Send offprint requests to: D. Barrado y Navascués, dbarrado@cfa.harvard.edu

^{*} Based on observations collected with the 2.2m telescope of the German-Spanish Observatorio de Calar Alto (Almería, Spain), and with the 2.56m Nordic Optical Telescope in the Spanish Observatorio del Roque de los Muchachos of the Instituto de Astrofísica de Canarias (La Palma, Spain)

crossing the giant gap or are in a later evolutionary stage, and their position in the Color-Magnitude Diagram does not allow to establish the evolutionary status (see Figure 1). To avoid confusion, we have named them here high luminosity (H-Lum) stars (compared with the other stars in this sample).

Paper II dealt also with the lithium abundances of those components on the MS or just evolving off it. We concluded that these stars have a Li excess, which could be related to their binary nature. In particular, we interpreted the excesses in the context of the transport of angular momentum between the orbit and the stars, which would inhibit mixing mechanism inside and lead to inhibition of Li depletion. Other scenarios, such as the depletion induced by internal gravity waves and the role of magnetic fields in inhibiting this process, can also be accommodated to the observations. We refer the reader to Paper I and Paper II for a detailed description of the properties of CABS and for an introduction to the Li depletion phenomenon among them. Additional information can be found in Fernández-Figueroa et al. (1993), Barrado y Navascués (1996) and Barrado y Navascués (1997).

In this work (Paper III), we study the Li abundances of evolved components of CABS, which provide complementary information to that obtained from dwarfs. In Section 2, we describe the data and the evolutionary status of our sample of stars, whereas Sections 3, and 4 contain the analysis and discussion of the lithium abundances. The conclusions are summarized in Section 5.

2. Program stars and observations

The basic data –namely, photometry, stellar masses, radii, distances, orbital and rotational periods– were selected from the Catalog of CABS (Strassmeier et al. 1993 and references therein). However, we revised the photometry for a significant fraction of the sample, carrying out a deconvolution of the photometry in order to locate each component in the Color-Magnitude Diagram and to compute accurate temperatures. Essentially, we used the available information to obtain colors and magnitudes for each component. Details about the process can be found in the footnotes of Table 1 and in Paper II. A more exhaustive study can be found in Barrado y Navascués (1996). Table 1 shows the systems which have been studied in this paper: column 1 lists the name of the system, column 2 the HD number, columns 3, 4, 5 and 6 the (U–B), (B–V), (V–R)_J and (V–I)_J colors, respectively, for each component. Column 7 lists the distance, whereas the 8th and 9th columns contain the apparent visual magnitude and the absolute magnitude computed with the previous 2 columns, respectively. In this last case, we also took into account other information in order to obtain the most accurate estimate of the magnitude of each component in the binary system (see notes in Table 1). Finally, column 10 declares if the system is SB1 or SB2, column 11 shows our evolutionary

classification: the bottom or the top part of the Red Giant Branch (B–RGB and T–RGB), and those stars with higher luminosity (H–Lum). This last case corresponds to components of CABS which are crossing for the first time the giant gap or are already burning helium, but due to their particular location in the CMD, it is not possible to determine the exact evolutionary stage. Column 12 provides the spectral type. The last column contains notes about the method used to compute the absolute visual magnitude and the photometric indices for each component (e.g., deconvolving the photometry. See Barrado y Navascués & Stauffer 1996). Note that the distances listed in Table 1 are pre-*Hipparcos*. We have preferred to maintain the previous values for coherence with Paper I and II. A revision of these results, together with new Li abundances derived from spectral synthesis, is in progress. In total, our sample has 70 systems, which contain 76 evolved components. A Color-Magnitude Diagram can be found in Figure 1. Note that we have used our deconvolved values of the photometry.

The observations were carried out in two different observing campaigns at the coudé focus of the 2.2m telescope of the Calar Alto Spanish-German Observatory (June 1993 and May 1994) and in an additional run at the 2.56m Nordic Optical Telescope of the Spanish Roque de los Muchachos Observatory (September 1994). In the first case, we used the Boller&Chivens spectrograph at the Coudé focus. For the last campaign, IACUB was utilized. This is a echelle spectrograph without cross dispersion. Since we used a filter to select the order around 6700 Å, no scatter light belonging to other order polluted our spectra.

Spectral resolutions ranged from 30,000 to 50,000 at λ 6700 Å. The spectra were reduced using standard procedures and the MIDAS¹ package. More details can be found in Paper II. Figure 2 shows a handful of our spectra. It can be appreciated their high quality. The signal-to-noise ratios range from 100 to 160.

3. Temperatures, lithium abundances, masses and ages

3.1. Effective temperature

The determination of the lithium abundances is strongly sensitive to the effective temperature. Therefore, we made real effort to try to derive them as accurately as possible (taking into account that these stars are binaries, and the observed photometry is the result of the combined light from both components). We used different color indices –namely, (B–V), (V–R), and (R–I), and computed the (V–I) using the last two indices–. First, we select the whole sample of CABS published in the Strassmeier et al. (1993) catalog. The deconvolution of the photometry

¹ Munich Image Data Analysis System is a program developed by European Southern Observatory, Garching.

was performed for the whole sample. Then, we computed different temperatures using the colors and the spectral type. The comparison between these values shows that the differences are quite small. In the case of the sample studied in this paper, the average temperature derived from $(V-I)_J$ and $(R-I)_J$ was selected for the cool component of each system, if these indices are known (temperature scales from Cayrel et al. 1985 and Carney 1983, respectively). For the hot components we used the calibration by Böhm-Vitense (1981), based on $(B-V)$. Although it depends on the availability of the data of different colors, in general the borderline is about 5000 K. We believe that this is the most accurate method to derive temperatures, since the contamination of light from the primary (hot component) is less in the red filters than in $(B-V)$. The spectral type and the Schmidt-Kaler (1982) scale were used for those components which do not have photometry accurate enough and to check the previous values. Results are listed in Table 2. The comparison between temperatures estimated using different calibrations does not show any relevant bias which could affect significantly the discussion performed in this work. The average value of the differences in temperatures (from the three color indices and the spectral type) is 110 K. Usual names, HD numbers, effective temperatures and radii, equivalent widths $-EW(Li+Fe)$ and $EW(Fe)$ as measured in this work and by Pallavicini et al. (1992)–, the final values of the lithium equivalent width $-EW(Li)-$, and comments can be found in this table, as well as the continuum correction factors (CCF). These last values take into account the contribution to the flux of each component and are very important to derive the actual equivalent widths. The CCF were determined using radii and temperatures of both components or, if the first ones were not available, from the visual magnitudes. We have also included all CABS studied by Pallavicini et al. (1992) and Randich et al. (1993, 1994) which were not observed during our observing runs.

3.2. Lithium abundance

The Li I doublet at λ 6708 Å is in fact a complex feature. At our resolutions, it appears as a single line and it could be blended with other spectral characteristics, either from the same star (like Fe I λ 6707.4 Å) or from the other component, since an important part of our systems are SB2. We measured the Li equivalent widths (EW) by fitting Gaussian curves to the relevant features, taking into account the phase information. Details of the procedure can be found in Paper II. Measured EW were corrected for the contribution to the continuum by the other component.

Table 3 lists the corrected lithium equivalent widths derived using the observed values and the CCF. It also includes four different lithium abundances: the values derived in this work, and those published by Pallavicini et al. (1992), and Randich et al. (1993; 1994). Other stellar pa-

rameters, such as masses, orbital and rotational periods, and an estimation of the age, appear in the last columns.

The final abundances were derived using the curves of growth of (CoG) Pallavicini et al. (1987). In order to reach lower temperatures, we added the CoG by Soderblom et al. (1993) corresponding to temperatures of 4000 and 4250 K and a gravity of $\text{Log } g=4.5$. To obtain abundances in the same way for the whole sample, using our temperatures and these curves of growth, we had to retrieve lithium equivalent widths from the published abundances by Randich et al. (1993; 1994). Since the comparison between the stars in common between these works and Pallavicini et al. (1992) shows that they are very similar, and this last study used the same CoG as us, we proceeded in the following way. First, using Randich et al. abundances and temperatures, we computed the equivalent widths. Second, with these values and our own temperatures, recalculated the abundances. As can be seen from the comparison of columns 5th, 6th, 7th and 8th, the abundances derived in most of the cases are quite similar. Essentially, the important departures appear when the temperatures selected by Pallavicini et al. (1992) and Randich et al. (1993; 1994) were very different from our values. In these cases, our temperatures are normally lower and, therefore, the abundances tend to be smaller.

The final errors in the Li abundances can be estimated as ~ 0.4 dex (see Paper II for details). In this case, there is an additional source of error for the abundances: the gravity. Pallavicini et al. CoG were computed for evolved and main sequence stars (we selected the appropriate set for each star), whereas Soderblom et al. CoG were obtained for main sequence stars. However, the comparison of the derived abundances for the same equivalent widths and temperatures and different gravity shows that the differences are negligible (~ 0.02) and they do not contribute in a significant way to the final errors.

3.3. Masses and ages

We selected the masses from the catalog of chromospheric active binaries by Strassmeier et al. (1993). In some cases, only the mass function has been published, but a value of the inclination has been obtained and it is possible to compute the mass. These cases are denoted with the flag “Msin³i” in column 9 of Table 3. Unfortunately, about half of the stars in this sample have unknown masses. The location of the component on the Radius-Teff plane and Color-Magnitude Diagram allows an estimate of the mass. For this goal, we used the Schaller et al. (1992) and Schaerer et al. (1993a,b) evolutionary tracks. The flags “RT” and “CM” indicate those masses derived by this way. It should be kept in mind that this is a crude estimation of the masses, since there are several factors that contribute to the uncertainty in the process. Among others, the errors in the parameters we used (temperature, radii, visual magnitude, color, distance), the set of evolutionary tracks (since

different metallicity shifts the positions and, therefore, a different mass is derived). In order to estimate the uncertainties of the the computed values, we have proceeded in the same fashion for those stars with known masses. The comparison between these values (the real ones and those from the CMD) shows that in general the agreement is good enough for low mass stars, in the range 1-3 M_{\odot} . However, more massive stars, as derived from the CMD, show, in general, larger values than the dynamic masses. The effect is more dramatic for those stars with masses around 5 M_{\odot} (CMD masses). An estimation of the error in the mass for this range is 2 M_{\odot} . For the low mass, it is about 20%. Thus, the high masses quoted in Table 3 with the flag ‘‘CM’’ should be taken with some caveats, since they are only intended as indicative value.

Ages were estimated following Paper I. We showed there that there is a clear correlation between mass and age for CABS. This relation can be used to estimate the age of those components whose radius is not known. In several cases, we assigned the age computed for the more massive component to the secondary, since the primary is the component which determines the evolutionary status of the system (the enhanced chromospheric emission arises normally from it). On the other hand, there are several systems which show clearly an anomalous evolution, with evidences of a significant transfer of material from one component to the other (e.g., a giant primary –brighter- with a main sequence as a secondary, having inverted mass ratios). Due to the complexity of the evolution of these systems, no age was estimated.

The actual expressions for evolved systems are:

$$\log \text{Age} = (9.81 \pm 0.04) - (2.64 \pm 0.10) \log (\text{Mass}/M_{\odot}), \text{ luminosity class III (1)}$$

$$\log \text{Age} = (10.00 \pm 0.02) - (3.25 \pm 0.10) \log (\text{Mass}/M_{\odot}), \text{ luminosity class IV (2)}$$

An illustration of these relations can be seen in Figure 3 of Paper I.

4. The dependence of lithium on several stellar parameters

4.1. Li abundance vs. effective temperature

In Figure 3a,b,c, we plot Li abundance against effective temperature. As it happens in members of open clusters, there is a clear trend between both quantities: the hotter the star, the larger the abundance. However, there is an important scatter and most of the evolved components of CABS have temperatures in the range 5000–4300 K and abundances $\log N(\text{Li}) \sim 0.5 - 1.2$ (in the customary scale where $\log N(\text{H})=12$). Similar plots for CABS have been produced recently by different authors (Pallavicini et al. 1992; Fernández-Figueroa et al. 1993; Randich et al. 1993, 1994), who concluded that a significant number of these stars have Li excesses, although it is not a characteristic as a group. This dependence between lithium abundance on

effective temperature is due to the fact that evolved components of CABS have changed their atmospheric physical parameters due to the evolution off the MS, cooling down due to the expansion of the external layers. A proper comparison between these stars and MS stars which are members of open clusters requires the knowledge of the stellar mass. As can be seen in Figure 3a, for the same temperature, there are stars which have very different mass (e.g., from 0.29 M_{\odot} to 5 M_{\odot}). Although these stars are in similar position in the $T_{\text{eff}}-\log N(\text{Li})$ plane, the mechanisms responsible for the Li depletion are completely different. Stars with masses larger than $\sim 1.5 M_{\odot}$, due to their shallow convective envelope, have not destroyed any photospheric Li during the MS life-time, whereas stars having masses in the range 0.8–0.9 M_{\odot} have burnt at least 99% of their original Li content at the age of M67 *before* they have left the MS (Chaboyer et al. 1995; Balachandran 1995; Barrado y Navascués et al. 1998). All of them, after they leave the MS phase, experiment a diminution of their photospheric Li due to the dilution process (see below), when the external layers are mixed with internal ones, poor in Li. Other mechanisms, such as turbulent circulation, could also be present at this stage. In addition, some CABS, with low orbital periods, have undergone a process of transfer of material when the primary has evolved off the MS.

Figure 3b contains comparison between our sample of CABS and giants belonging to open clusters (Gilroy 1989). The binaries are shown as solid symbols and the cluster giants appear as open circles. The ages of the clusters range from 5×10^7 to 2×10^9 yr. No obvious difference can be concluded from this plot. For the area in common between both groups, the distribution of lithium abundances is quite similar and any difference could be attribute to the differences in the analysis and/or to the uncertainties of ages and abundances. A more meaningful comparison is carried out in Figure 3c. We selected a those CABS having masses in the range $1.1 \leq \text{Mass} \leq 1.5 M_{\odot}$ (solid symbols). The open circles represent single, evolved M67 stars (Barrado y Navascués et al. 1998). The lithium abundances in both samples were derived in similar way, using the same set of CoG. The M67 members have masses around 1.3 M_{\odot} , as derived from the CMD. Most of these stars have only upper limits for the lithium abundances. The visual inspection of the figure indicates that the abundances are systematically larger in the case of the CABS (half of them have an abundance about 0.6 dex larger than the values of the M67 members for the same temperature). However, it should be kept in mind that the masses of the CABS cover a larger range and that the M67 giants could come from MS stars in the Li gap.

4.2. The mass–log $N(\text{Li})$ plane

Knowledge of the stellar masses of evolved components of CABS allows us to avoid the evolutionary effects when

comparing Li abundances. Figure 4 shows Li abundance against mass. Components at the bottom of the RGB are represented as open circles, whereas those at the top of the RGB appear as solid squares, and giants belonging to the H-Lum are shown as open triangles. The average Li abundance of single Hyades stars and the predicted abundances for subgiant and giant stars due to dilution (Iben 1966, 1967a,b; after Scalo & Miller 1980) are included as a solid line. This process was described originally by Iben (1965) and appears when a star evolves off the MS. When it crosses the giant gap and climbs the RGB, the convective envelope increases its fraction in mass. Material poor in Li arises to the surface and is mixed with Li-rich material. This process stops when the star achieves the maximum size of its convective envelope, but the depletion of the surface Li can continue if there is a further mixing related to rotation (Ryan & Deliyannis 1995). With the exception of three stars, the rest of the sample objects have abundances at least 1 dex lower than the “cosmic” value (dashed line at $\log N(\text{Li})=3.2$; Martín et al. 1994), indicating that they have suffered Li depletion and/or dilution (in this last case, as the star to ascent the RGB). One of these three stars is in the middle of the Li gap (Boesgaard & Tripicco 1986a,b) and two of them (HR5110 and α Aur) have signs of an anomalous evolution (see Paper I) and/or seem to be first crossing the giant gap.

Several stars have lithium abundances between the cosmic value and the values predicted by dilution. However, they are either massive stars (H-Lum or T-RGB) in an ambiguous evolutionary stage or stars classified as B-RGB, but at the beginning of the evolution in the RGB. Therefore, their high lithium abundances could be explained as a result of a limited lithium dilution, since the convective envelope has just started to expand inwards. However, other mechanisms could be acting (see below).

Two thirds of the stars in the sample have abundances below the dilution limit. However, this is a maximum value, since MS experiment lithium depletion before they evolve off it, and a further depletion could take place later. Brown et al. (1989) showed that $\sim 99\%$ of the large sample of giants studied by them have a lithium abundance well below the predicted abundances due to the mixing process during the first dredge-up. In particular, the average abundance is $\langle \text{Log } N(\text{Li}) \rangle_{\text{giant}} \leq 0.0$. However, less than a dozen components of CABS have similar abundances to the field giants, and most of the stars in our sample have values clearly above them.

On the other hand, when the comparison is made for stars in the same mass range, some T-RGB stars have abundances higher than those characteristic of B-RGB, which are in a evolutionary stage previous to that corresponding to T-RGB. A similar situation appears if the comparison is made between T-RGB and H-Lum stars (but in this case, some H-Lum could be crossing the giant gap for the first time). Since evolved stars become older as they climb the RGB or the asymptotic giant branch

(AGB), it seems that part of the evolved stars in our sample have a Li abundance which does not depend on age or evolutionary stage. This conclusion, derived from a comparison of abundances, masses and luminosity classes, is the same as that one obtained from the study of ages (see next section).

The scatter of massive stars ($\sim 5 M_{\odot}$) is remarkable: the Li abundances vary in 2.5 dex. Brown et al. (1989), using a large sample of giant stars, showed that only about 2% among them have Li abundances higher than $\log N(\text{Li})=1.5$ and a 7.6% larger than 1.0 dex, in good agreement with the theoretical predictions based on the dilution. However, the lithium abundances of the massive stars in our sample follow a complete different pattern. Since these stars seem to have the similar masses (the uncertainties are large for most of them) and are in the same evolutionary stage, it seems that some have retained the lithium at the maximum level predicted by dilution, whereas others have depleted it (the maximum difference is 1.8 dex). Note that almost all of them have abundances larger than the stars studied by Brown et al. (1989). Sackmann & Boothroyd (1995) have shown that circulation processes in AGB stars can transport material and can explain the high Li abundances and the low $^{12}\text{C}/^{13}\text{C}$ ratios found in these stars (a low $^{12}\text{C}/^{13}\text{C}$ ratio indicates a deep mixing). These abundances would be produced in layers at high temperatures close to the core in stars with masses in the range 4–7 M_{\odot} in the so called “hot bottom burning”, and would be transported to the surface during the second dredge-up via deep circulation. Moreover, this transport would be effective also for stars in the RGB, with inferior masses. Li would be created via the Cameron-Fowler mechanism (“cool bottom processing”) in the layer where H is burned. In this mechanism, Be would be first synthesized due to interactions between ^3He and ^4He . This new material would be rapidly transported toward the exterior, due to deep circulation, where Li would be created by electronic capture. However, this scenario does not explain the large scatter in the Li abundances of stars in the same evolutionary stage and should be acting in normal stars. Only if the deep circulation responsible of the transport of the Be to the external layers would depend on rotation, this mechanism could be used as an explanation for the lithium excesses. Fekel & Balachandran (1993) established that single giants with strong stellar activity have large Li abundances and suggested that these abundances could be related to transport of angular momentum and material from the interior to the surface. They have interpreted that, when these stars expand their convective envelopes inwards while ascending the RGB, they transport angular momentum toward the surface and new synthesized Li from the nuclear reactions $^3\text{He}(\alpha, \gamma)^7\text{Be}(e, \nu)^7\text{Li}$ (Simon & Drake 1989). This scenario is fraught with problems as well. It presupposes a reservoir of angular momentum in the stellar interior. This reservoir must be large enough to spin up the surface of a

giant and the cause of the angular momentum dredge-up is unknown. Our results show that some active stars do have larger abundances. However, we have only found a trend between rotation and lithium excesses, and if there is any clear connection (see next section), it should be very subtle (such as a dependence in the rotational story as the component evolve off the MS and ascent the RGB, very complex in close binaries due to the evolution of the convective envelope and the transport of angular momentum). Therefore, these data cannot discriminate directly between these scenarios.

Some components with masses $\sim 2.5 M_{\odot}$ have Li abundances close to the cosmic value. This fact would indicate that, despite that they have expanded and developed convective envelopes, they have not mixed the external material, Li-rich, with the internal one, without it. Lithium could have been diffused upwards during the pre-main sequence phase and would have achieved such high concentrations in the surface Li-preservation zone that subsequent red giant dilution decreased the Li only by a factor of 2–3 with respect to the cosmic value. Since the expected dilution is a factor of about 50, the diffused concentrations must be nearly a factor of 25 above cosmic. Such large surface abundances ($\log N(\text{Li}) \sim 4.5$) have never been reported in main sequence stars, and thus this concentrated layer of Li must lie below the surface convective zone but in the Li-preservation zone, a difficult theoretical feat. An alternative explanation would be Li creation in the stellar interior. For this mass range, Fekel & Balachandran (1993) also found that a large fraction of chromospherically active giants have high Li (See above). However, the simplest explanation is to assume that they have diluted partially the lithium due to the fact that they have just started to climb the RGB.

Some of the low mass stars ($\sim 1 M_{\odot}$) have abundances larger than the maximum values predicted by dilution, but under the average values of Hyades MS stars ($\log N(\text{Li}) = 0.4\text{--}1.0$ dex). Since most of the original Li is depleted in single stars during the MS (e.g. Chaboyer et al. 1995), either a little amount of Li has been destroyed after the evolution off the MS, as happens in MS components of CABS (Paper II), or a mechanism has prevented the depletion during the present phase of the stellar evolution.

Randich et al. (1993, 1994) found that a significant number of evolved CABS have Li excesses with respect to the typical values observed in other evolved stars of similar spectral types. They pointed out that the most plausible interpretation was that the CABS have evolved from massive progenitors ($M > 1.5 M_{\odot}$), who have suffered little or no depletion on the MS. However, they did not find the expected correlation between the Li abundances and the masses. In our case, we have not found this trend either. Moreover, the spread in the Li abundances for stars at the same mass range and the obvious Li excesses in some stars with masses smaller than $1.5 M_{\odot}$ are strong indica-

tions that others mechanisms are acting, and inhibiting partially the Li depletion for some CABS.

From this diagram, we conclude that there are some indications of inhibition of the Li depletion as it happens in MS components of CABS (Paper II). However, these lithium excesses are very small, and the inhibition of the depletion seems to be only partial. Moreover, they are only present in a fraction of the sample of evolved components of CABS.

4.3. Lithium and age

Using theoretical isochrones and the age–mass relationship, we have estimated the ages of evolved components of CABS (Section 3.3). The comparison between these ages and the Li abundances indicates that there is no relation between them. Figure 5 displays the CABS as circles (the size increases with the mass). As a comparison, we have included giant stars –solid diamonds– belonging to several open clusters of different ages from Gilroy (1989). For any particular mass range, there is an important dispersion of $\log N(\text{Li})$ and a lack of dependence with age.

In particular, stars having masses in the range $3.0 > M/M_{\odot} > 2.0$ have a large spread in a very small age range. However, once the secondaries (the less massive star in the system) and 6 Tri, whose mass is uncertain, are removed, the spread is reduced by a large amount, except for HR1023. Since this group of stars has not depleted its initial Li content during the Pre-main Sequence (PMS) or MS stages, the value should be around $\log N(\text{Li}) = 1.5$ or less, the maximum value permitted by dilution, as it happens with the observed abundances.

In the case of the stars having masses in the range $1.2\text{--}1.6 M_{\odot}$, the dispersion could be explained due to the fact that these stars come from mid F-type stars in the MS (the stars located in the Li gap, where the Li content can decrease by 2 dex before the star evolves off the MS). The observed Li dispersion hardly depends on rotation, because although rotation inside the MS could cause a dispersion, after the stars evolved off the MS this information is lost due to the transport of angular momentum from the interior to the surface. However, as shown in Figure 3a, these stars do have Li excesses.

Finally, stars with masses lower than $1.2 M_{\odot}$ show abundances similar to those characteristics of stars from open clusters. A very close look reveals that evolved components of CABS with masses in the range $0.8\text{--}0.9 M_{\odot}$ have Li abundances higher than equivalent stars member of open clusters, in the same way of MS components of CABS (Paper II).

4.4. Lithium and rotation

Figure 6a shows Li abundance against the photometric period of CABS. Symbols are as in Figure 3a, and the size of the symbols increases with mass. There is a trend between

both quantities, although a large scatter is also present which does not disappear if a particular mass range is selected. In any case, it is obvious that there are no systems with large values of both photometric period and Li abundance.

Observations of unevolved late-type stars in young open clusters like α Persei and the Pleiades indicate that there is a dependence of Li abundance on rotation: the most rapid rotators are generally the most Li-rich objects and exhibit a much narrower abundance dispersion than the slow rotators (García López et al. 1994; Randich et al. 1998). De Medeiros et al. (1997) have found, analyzing 65 subgiants of spectral types F, G and K, that there is a correlation between $v \sin i$ and $\log N(\text{Li})$, but only for single stars. They also found discontinuities in both parameters for stars of spectral type F8 IV $-(B-V) \sim 0.55$. Since the magnetic braking seems to be responsible for the rotational discontinuity, this work argues that the magnetic braking can also produce the discontinuity in the Li abundance. In our case, there are no such discontinuities. The orbit supplies angular momentum to replace that one lost via magnetic braking and we have not observed any discontinuity in the $T_{\text{eff}}-\log N(\text{Li})$ plane. Again, rotation and evolution seem to be important factors in the Li depletion phenomenon.

The particular way rotation influences the evolution of Li in evolved stars is not clear. If transfer of angular momentum between the orbit and the rotation inhibits the mixing process below the convective envelope, the Li abundance should be larger in systems having short orbital periods, since P_{orb} would be coupled to the rotation due to tidal forces. However, several asynchronous systems have large abundances (TY Pic, HR3385, 93 Leo, HR6469, AS Cap) and, as a group, there is no difference in the behavior of the Li abundances between systems with and without synchronization (Figure 6b). On the other hand, there is a trend between the temperature and the photometric period. Therefore, it is not clear the link between rotation and Li abundances. As we pointed out before, Fekel & Balachandran (1993) have found that, in chromospherically active giants, high rotation is connected with high Li abundance. This mechanism is likely not acting in CABS since it seems to appear only in AGB stars, more massive and in a more evolved evolutionary stage than CABS.

Our interpretation of the high Li abundances of several CABS involves the normal evolution of rotation and internal structure. When a star crosses the giant gap, the core decreases its size while the convective envelope increases. The conservation of angular momentum induces a shear effect between the core, which rotates faster and faster, and the envelope, which is decreasing its rotation rate. The effect would be a mix related to rotation which would cause transport of Li well below the convective envelope and its annihilation. Therefore, the Li abundances would be smaller than those predicted by dilution, showing a scat-

ter which depends on the initial angular momentum. In the case of CABS, and specifically for those systems which have been synchronized during the MS or when they have evolved off the MS (tidal forces depend on the size of the convective envelope and stellar radius), the orbit acts as a source of angular momentum to the rotation, avoiding the differential rotation between the core and the convective envelope, and the turbulent mixing, keeping more Li than single stars at the same evolutionary stage. If this mechanisms were responsible for the observed abundances, the stellar rotational history (including the evolution of orbital and rotational periods) would be very important in the way Li evolves with time but, unfortunately, this is an information lost at this evolutionary stage.

5. Summary and conclusions

We have studied the lithium abundances of evolved components of CABS. As it happens in late-type stars belonging to open clusters, there is a relation between the Li abundance and the effective temperature, although a very large scatter is present. Since these stars have different masses (even in the case of the same T_{eff}), various mixing mechanisms should be working.

We have found that some evolved components show partial inhibition of the Li destruction, and there are several cases with abundances above the maximum value predicted by dilution. Part of these stars have Li abundances which do not depend on the age or the evolutionary stage. In particular, there is a very large scatter for those stars having $\sim 5 M_{\odot}$, which could indicate that the circularization process proposed for AGB stars or creation of Li via the Cameron–Fowler mechanism are acting. They could also be due to the transport of material associated with the transport of angular momentum, but our data cannot discriminate between them.

A Li abundance spread also appears in groups of the same age and mass. This scatter is related to rotation, but the particular way stellar rotation influences the Li abundance in evolved components of these binaries is not clear. However, the transfer of angular momentum from the orbit to the rotation in the Main Sequence and when the stars are evolving off it could inhibit partially the mixing of material (and the dilution) and the destruction of Li associated with it. However, the problem is still unsolved and more work is needed to understand how Li evolves in low-mass evolved stars and, in particular, in binary systems of different types.

Acknowledgements. This research has made use of the Simbad database, operated at CDS, Strasbourg, France. We greatly appreciate the comments and suggestions on this paper by the referee, Dr. Sofia Randich, which helped to improve the presentation and discussion of the results. DBN acknowledges the support by the Universidad Complutense, the Real Colegio Complutense at Harvard University, and the MEC/Fulbright commission. This work has been partially supported by the

Spanish Dirección General de Educación Superior (DGES) under projects PB92-0434-C02-01, PB94-0203, and PB95-1132-C02-01.

References

- Balachandran, S., 1995, *ApJ* 446, 203
- Barrado, D., Fernández-Figueroa, M. J., Montesinos, B., De Castro, E., Cornide, M., 1994, *A&A* 290, 137 (Paper I)
- Barrado y Navascués, D., 1996, Ph. D. Thesis. Universidad Complutense de Madrid
- Barrado y Navascués, D., 1997, *PASP* 109, 70
- Barrado y Navascués, D., Fernández-Figueroa, M.J., García López, R.J., de Castro, E., Cornide, M., 1997, *A&A* 326, 788 (Paper II)
- Barrado y Navascués, D. and Stauffer, J.R., 1996, *A&A* 310, 879
- Barrado y Navascués, D., Stauffer, J.R., Hartmann, L., Balachandran, S., 1998, *Mem.S.A.It* (in press)
- Boesgaard, A. M., and Tripicco, M.J., 1986a, *ApJ* 302, L49
- Boesgaard, A.M., and Tripicco, M.J., 1986b, *ApJ* 303, 724
- Böhm-Vitense, E., 1981, *ARA&A* 19, 295
- Brown, J.A, Sneden, C., Lambert, D.L., Dutchover, E.Jr., 1989, *ApJS* 71, 293
- Carney, B.W., 1983, *AJ* 88, 623
- Cayrel, R., Cayrel de Strobel, G., Campbell, B., 1985, *A&A* 146, 249
- Chaboyer, B., Demarque, P., Pinsonneault, M.H., 1995, *ApJ* 441, 876
- De Medeiros, J.R., Do Nascimento, Jr., Mayor, M., 1997, *A&A* 371, 701
- Fernández-Figueroa, M. J., Barrado, D., De Castro, E., Cornide, M., 1993, *A&A* 274, 373
- García López, R. J., Rebolo, R., Martín, E. L. 1994, *A&A* 282, 518
- Gilroy, K., K., 1989, *ApJ* 347, 835
- Iben, I., 1965, *ApJ* 142, 1446
- Iben, I., 1967, *ApJ* 143, 483
- Iben, I., 1967a, *ApJ* 147, 624
- Iben, I., 1967b, *ApJ* 147, 651
- Pallavicini, R., Cerruti-Sola, M., Duncan, D.K., 1987, *A&A* 174, 116
- Pallavicini, R., Randich, S., and Giampapa, M. S., 1992, *A&A* 253, 185
- Randich, S., Gratton, R., Pallavicini, R., 1993, *A&A* 273, 194
- Randich, S., Gratton, R., Pallavicini, R., 1994, *A&A* 283, 893
- Randich, S., Martín, E. L., García López, R. J., & Pallavicini, R. 1998, *A&A* (in press)
- Ryan, S.G. and Deliyannis, C.P., 1995, *ApJ* 453, 819
- Sackmann, I-J., Boothroyd, A.I., 1995, *Mem.S.A.It* 66, 403
- Scalo, J.M., Miller, E.M., 1980, *ApJ* 239, 953
- Schmidt-Kaler, T., 1982 in: Landolt-Börnstein, Vol. 2b, eds. K. Schaifers, H. H. Voig. Springer, Heidelberg
- Soderblom, D.R., Jones, B.F., Balachandran, S., Stauffer, J.R., Duncan, D.K., Fedele, S.B., Hudon, J.D., 1993, *AJ* 106, 1059
- Strassmeier, K.G., Hall, D.S., Fekel, F.C., Scheck, M., 1993, *A&AS* 100, 173

Figure 1.- Color-Magnitude diagram for our sample of evolved CABS. Note that we have used the deconvolved photometry.

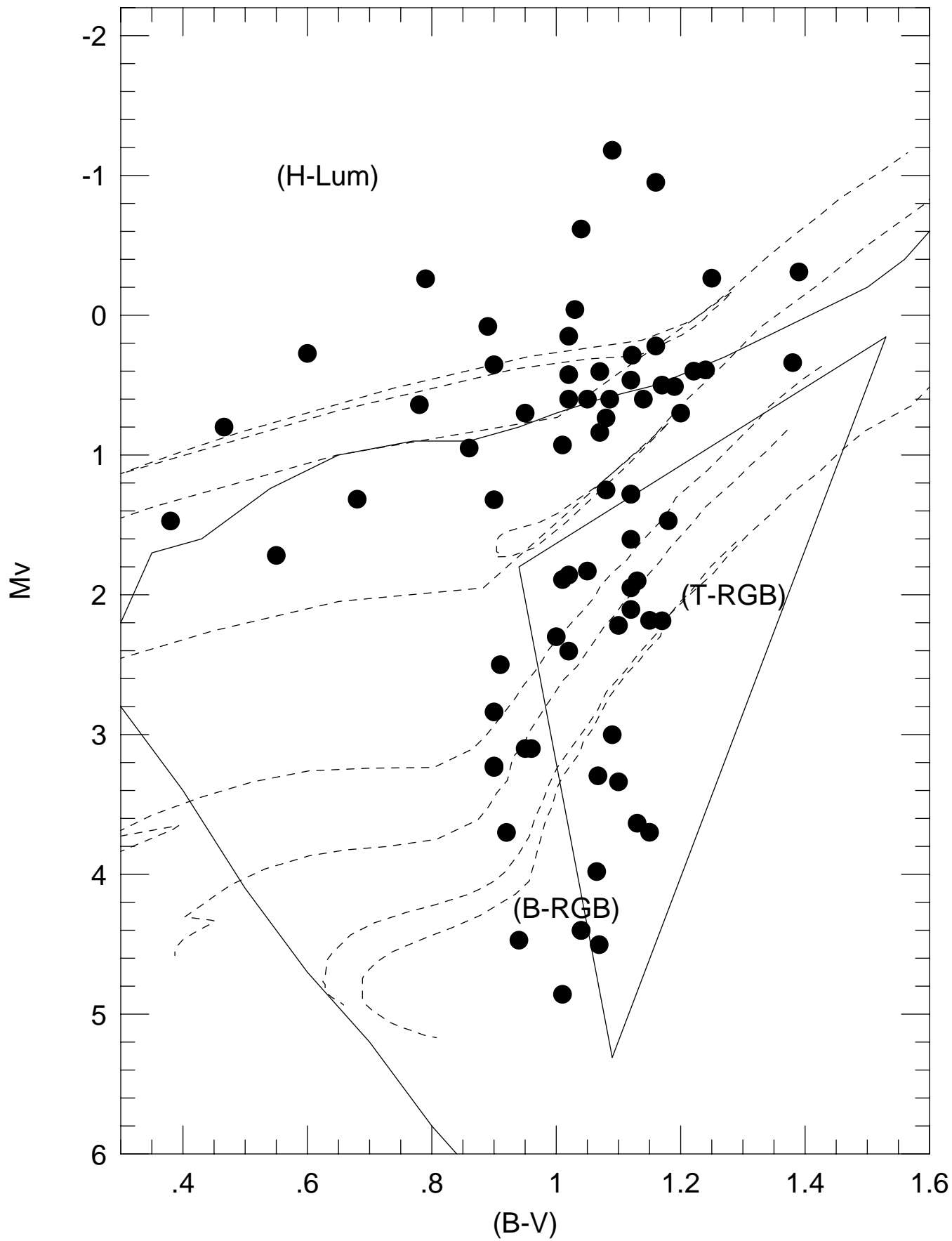
Figure 2.- Several examples of the spectra.

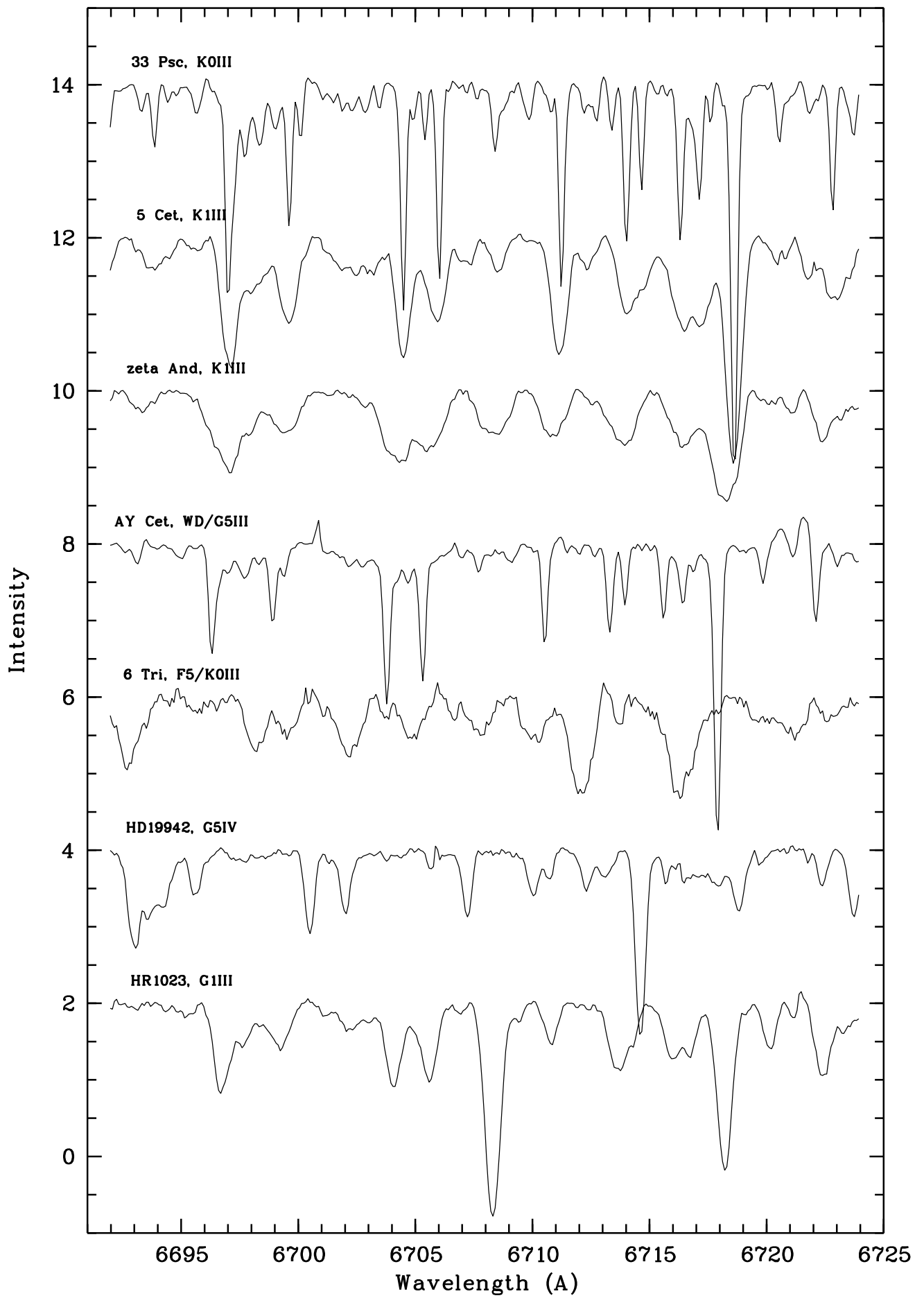
Figure 3.- Lithium abundance against effective temperature. **a** Giant components of CABS are shown as circles, and the size increases with stellar mass. **b** Comparison between the CABS (solid circles) and giant members of open clusters (open circles). **c** Comparison between CABS in the mass range $1.1 \leq \text{Mass} \leq 1.5 M_{\odot}$ (solid circles) and giants belonging to M67 (open circles).

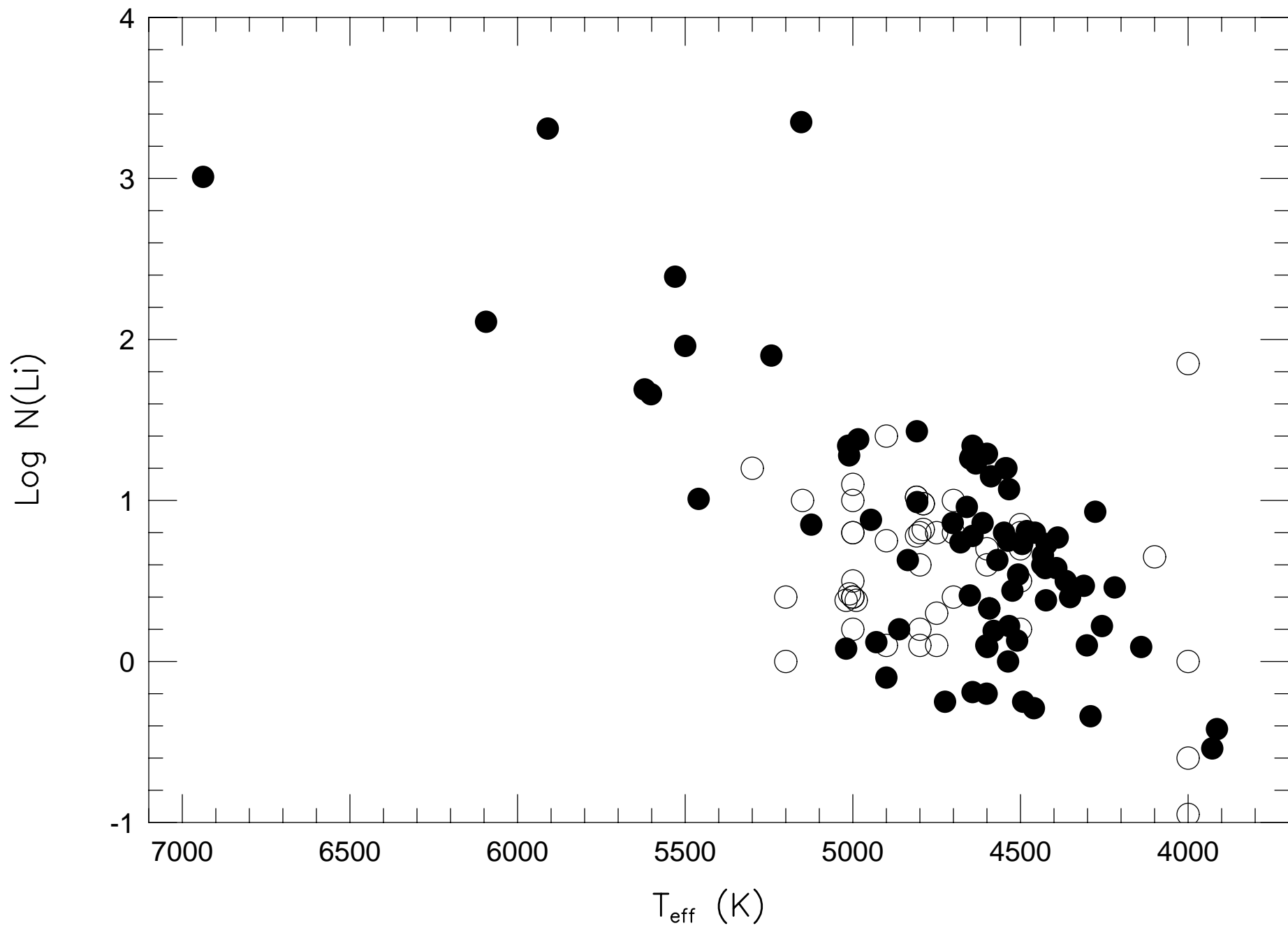
Figure 4.- Lithium abundance against stellar mass. The average Li abundances of Hyades stars and the maximum abundance predicted by dilution are shown as a solid lines. The cosmic abundance appears as a dashed line.

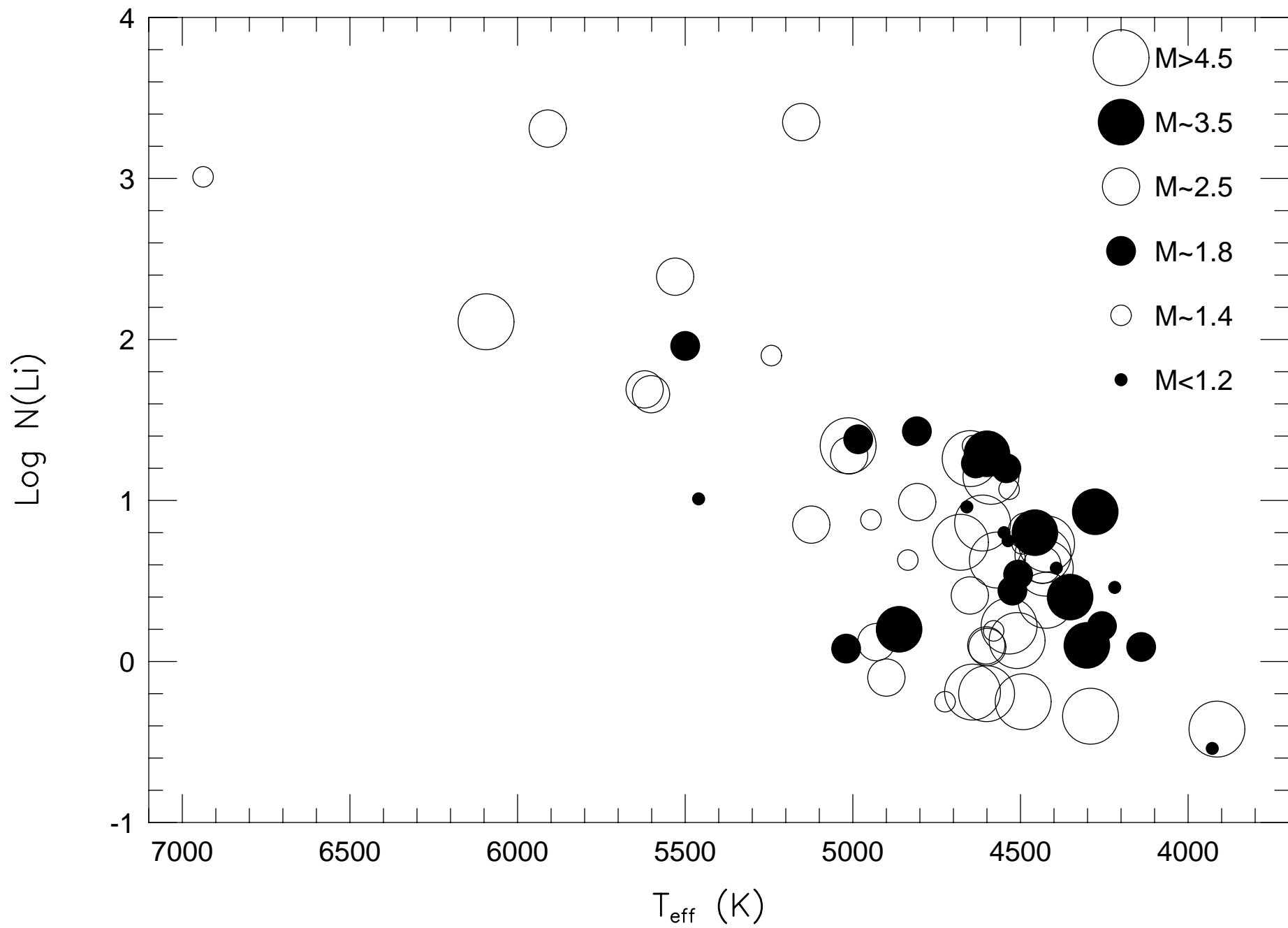
Figure 5.- Li abundance against stellar age. Sizes of the circle symbols increase with increasing stellar mass. Cluster giants are shown as solid diamonds.

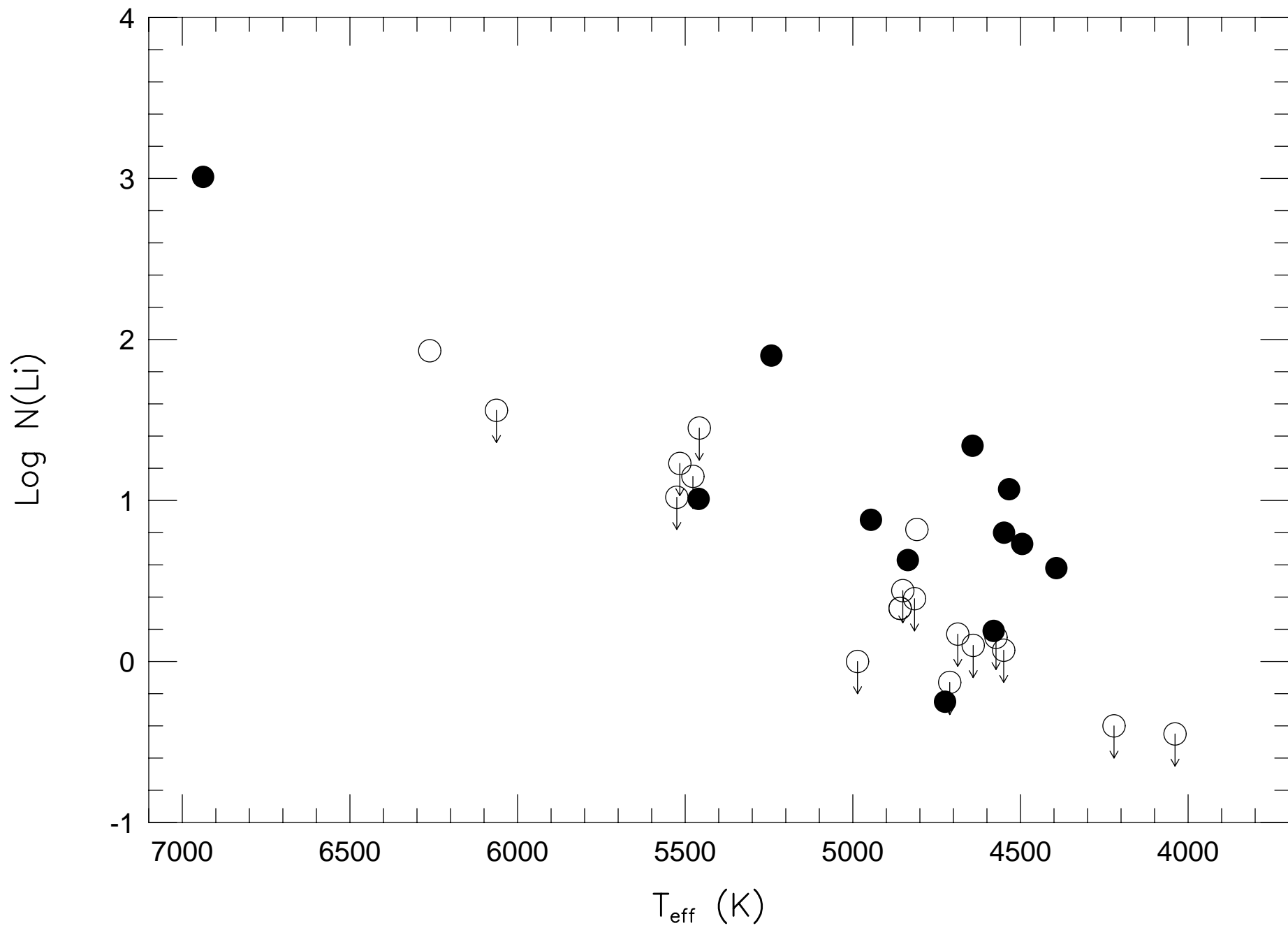
Figure 6.- Relation between Li abundances and the photometric periods. **a** Size increases with stellar mass. **b** Synchronous and asynchronous systems (solid and open circles, respectively).

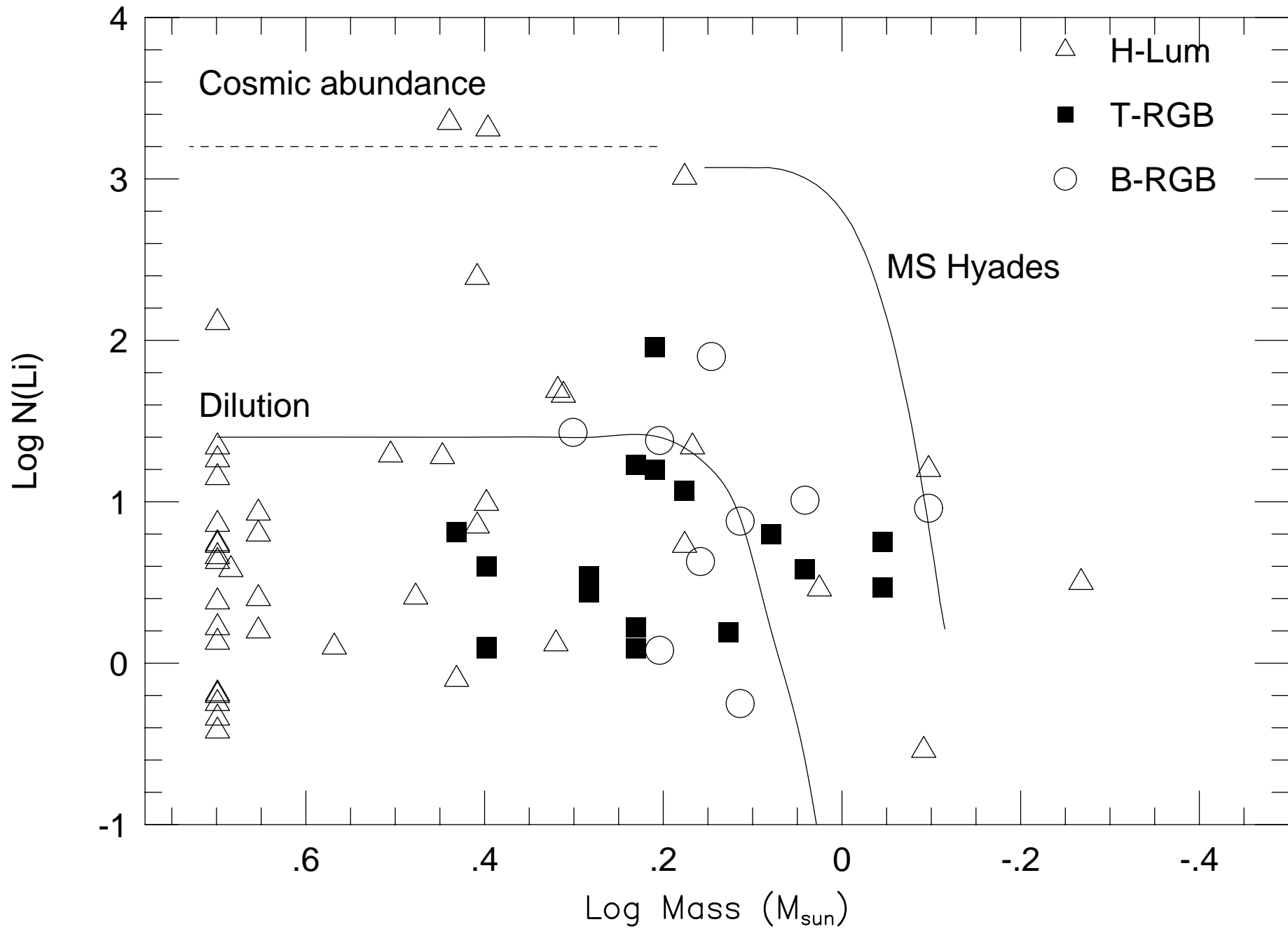


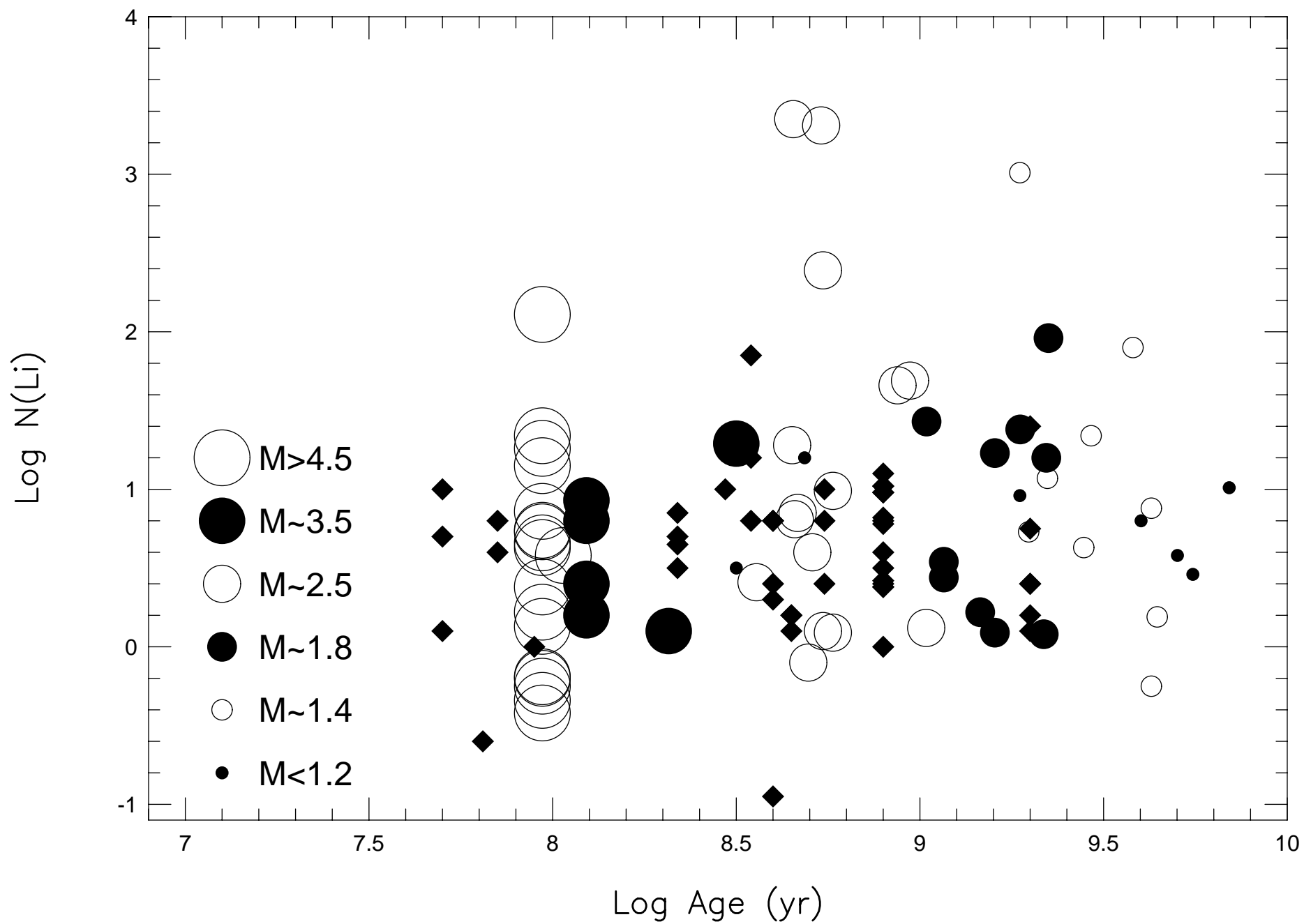


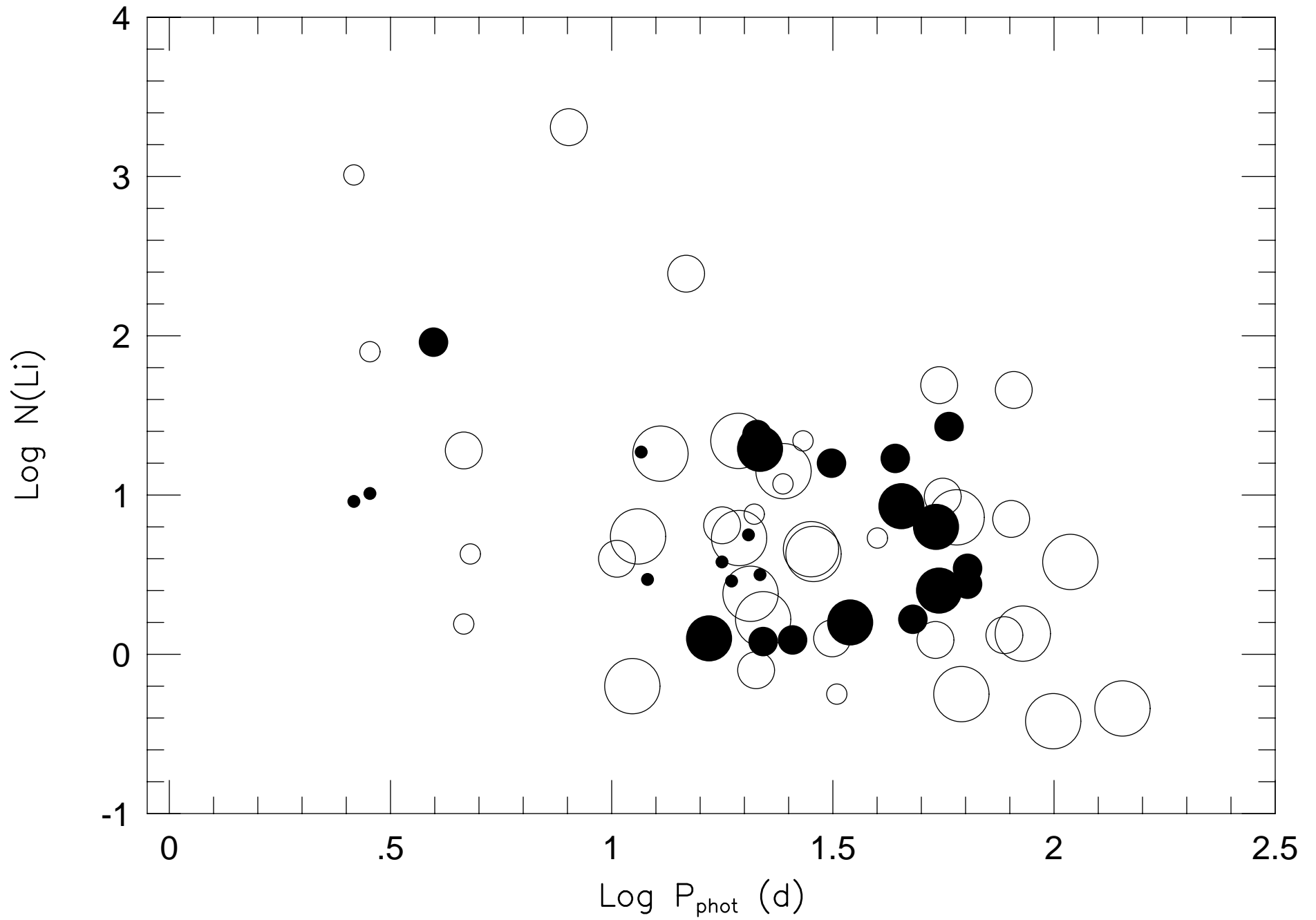












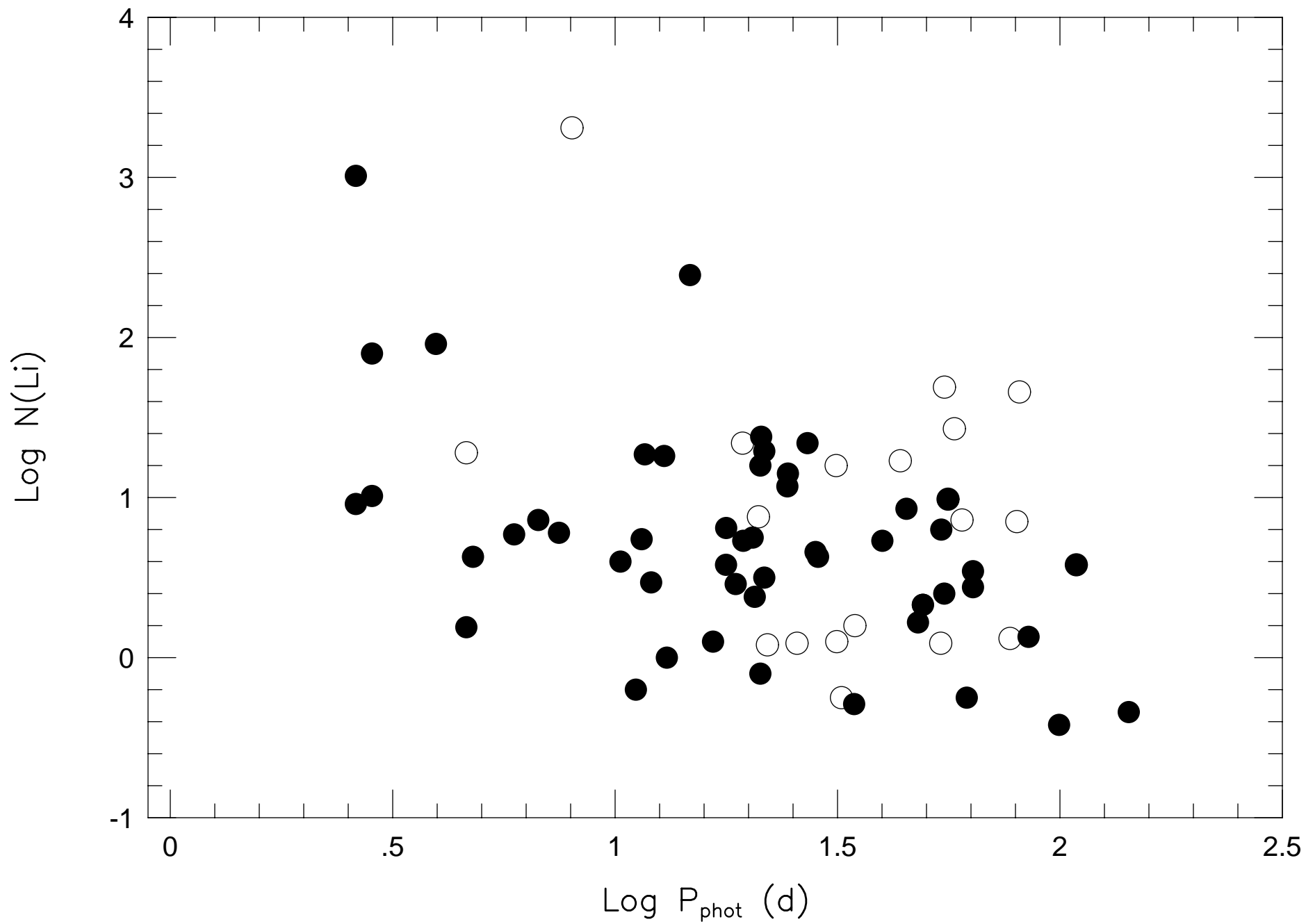


Table 1: Photometry of our sample of CABS containing evolved stars

Name (1)	HD (2)	(U-B) (3)	(B-V) (4)	(V-R) _J (5)	(R-I) _J (6)	D (pc) (7)	V (8)	Mv(d,V) (9)	SB (10)	Status (11)	Sp.type (12)	Comments (13)
33 Psc	28	0.890	1.040	–	0.540	111.0	4.610	-0.617	1	H-lum	K0III	a
5 Cet	352	–	–	–	–	140.0	–	–	1	MS	wF	
5 Cet	352	1.140	1.380	–	–	140.0	6.070	0.339	1	H-lum	K1III	a
BD Cet	1833	0.960	1.130	0.690	0.595	71.0	7.890	3.634	1	T-RGB	K1III	a,kc
zeta And	4502	0.900	1.120	0.840	0.590	31.0	4.060	1.603	1	T-RGB	K1III	a
AY Cet	7672	–	–	–	–	66.7	–	–	1	WD	WD	
AY Cet	7672	0.570	0.900	0.690	–	66.7	5.470	1.320	1	H-lum	G5III	a
UV For	10909	0.610	0.960	0.780	0.524	–	7.970	3.1	1	B-RGB	K0IV	a,kc,j
6 Tri	13480	–	–	–	–	75.0	–	3.5	2	MS	F5	j
6 Tri	13480	–	0.780	–	–	75.0	4.940	0.640	2	H-lum	K0III	a,i
EL Eri	19754	0.740	1.120	0.940	0.640	–	7.920	1.95	1	T-RGB	G8IV-III	a,j
BD+43 657	19942	–	0.900	–	–	65.0	7.300	3.235	1	B-RGB	G5IV	a
HR 1023	21018	0.510	0.860	–	–	–	6.380	0.95	1	H-lum	G1III	a,j
V711 Tau	22468	0.460	–	–	–	36.0	–	4.2	2	B-RGB	G5IV	c,k
V711 Tau	22468	–	0.920	0.770	0.390	36.0	–	3.7	2	B-RGB	K1IV	a,d,k
HR 1176	23838	0.152	–	–	–	–	–	3.6	2	MS	F2V	c,j
HR 1176	23838	–	0.466	–	0.290	–	5.660	0.8	2	H-lum	G8III	a,j
V492 Per	28591	–	0.900	–	–	50.0	6.720	3.225	1	B-RGB	K1III	a
3 Cam	29317	0.890	1.070	–	–	85.0	5.050	0.403	1	H-lum	K0III	a
RZ Eri	30050	0.260	0.430	–	–	143.0	–	3.48	2	MS	Am	
RZ Eri	30050	0.680	1.100	–	–	143.0	7.700	2.219	2	T-RGB	K0IV	f
12 Cam	32357	–	1.120	–	–	134.0	6.100	0.464	1	H-lum	K0III	a
CP-77 196	34802	0.790	1.090	0.863	0.564	82.0	7.570	3.001	1	T-RGB	K1IIIp	a,kc
alpha Aur	34029	–	0.600	–	–	13.0	–	0.273	2	H-lum	G1III	m
alpha Aur	34029	0.440	0.900	–	0.440	13.0	–	0.354	2	H-lum	K0III	a,d,e,m
TW Lep	37847	–	–	–	–	220.0	–	2.6	2	MSoff	F6IV	j
TW Lep	37847	0.740	1.020	0.891	0.585	220.0	7.000	0.425	2	H-lum	K2III	a,kc,i
V1149 Ori	37824	0.900	1.140	0.900	0.580	–	6.580	0.6	1	H-lum	K1III	a,j
TY Pic	42504	–	–	–	–	110.0	–	–	1	MS	F	
TY Pic	42504	0.670	1.020	0.808	0.544	110.0	7.610	2.403	1	T-RGB	G8-K0III	a,kc
TZ Pic	46697	1.000	1.150	0.877	0.554	60.0	7.590	3.699	1	T-RGB	K1IV-IIIp	a,kc
AR Mon	57364	–	–	–	–	525.0	–	0.85	2	H-lum	G8III	h
AR Mon	57364	–	1.080	–	–	525.0	–	1.25	2	H-lum	K2-3III	a,d,e,h
V344 Pup	61245	0.810	1.050	0.794	0.534	–	6.880	0.6	1	H-lum	K1III	a,kc,j
sigma Gem	62044	0.937	1.122	0.920	0.580	59.0	4.140	0.286	1	H-lum	K1III	a
LU Hya	71071	0.670	0.950	0.738	0.472	–	7.340	3.1	1	B-RGB	K1IV	a,kc
HR 3385	72688	0.660	0.950	0.710	0.462	–	6.320	0.7	1	H-lum	K0III	a,kc,j
RZ Cnc	73343	–	–	–	–	395.0	–	1.331	2	H-lum	K1III	m
RZ Cnc	73343	–	1.180	–	–	395.0	–	1.470	2	H-lum	K3-4III	a,d,m
IL Hya	81410	0.700	1.020	0.790	0.550	263.0	7.250	0.150	1	H-lum	K1III	a
IN Vel	83442	1.000	1.170	0.919	0.605	–	8.830	0.5	1	H-lum	K2IIIp	a,kc,j
DM UMa	–	–	1.065	–	–	130.0	9.550	3.980	1	T-RGB	K0-1IV-III	a
CD-38 7259	101309	–	–	–	–	62.0	–	5.1	2	MS	G5V	j
CD-38 7259	101309	0.480	0.940	0.780	0.554	62.0	7.950	4.471	2	B-RGB	K1IV	a,kc,i
HR 4492	101379	0.260	–	–	–	140.0	–	0.65	1	MS	A0	a,j
HR 4492	101379	–	0.790	0.630	0.554	140.0	5.080	-0.261	1	H-lum	K2-4III	a,kc,i
93 Leo	102509	–	–	–	–	36.0	–	2.075	2	MS	A6V	j
93 Leo	102509	0.280	0.550	–	0.360	36.0	4.500	1.718	2	H-lum	G5IV-III	a
HU Vir	106225	0.660	1.020	0.866	0.598	220.0	8.570	1.858	1	T-RGB	K0IV	a,kc
HR 4665	106677	–	1.120	0.890	0.560	130.0	6.893	1.280	2	T-RGB	K1III	b
HR 4665	106677	–	1.120	0.890	0.560	130.0	6.893	1.280	2	T-RGB	K1III	b
BD-04 3419	113816	–	1.150	0.930	0.540	165.0	8.270	2.183	1	T-RGB	K2IV-III	a
RS CVn	114519	0.090	0.420	–	–	180.0	–	2.6	2	MSoff	F4IV	c,h
RS CVn	114519	–	0.910	0.720	–	180.0	–	2.5	2	B-RGB	G9IV	a,d,h
BM CVn	116204	1.000	1.160	–	–	250.0	7.210	0.220	1	H-lum	K1III	a
HR 5110	118216	0.050	0.380	0.407	0.190	53.0	4.930	1.472	2	H-lum	F2IV	a,i
HR 5110	118216	–	–	–	–	53.0	–	3.45	2	B-RGB	K2IV	j
V851 Cen	119285	0.819	1.067	0.919	0.626	80.0	7.810	3.295	1	T-RGB	K2IV-III	a,kc
V841 Cen	127535	0.794	1.069	0.898	0.605	63.0	8.500	4.503	1	T-RGB	K1IV	a,kc

Table 1: (continued)

Name	HD	(U-B)	(B-V)	(V-R) _J	(R-I) _J	D (pc)	V	M _V (d,V)	SB	Status	Sp.type	Comments
(1)	(2)	(3)	(4)	(5)	(6)	(7)	(8)	(9)	(10)	(11)	(12)	(13)
UV CrB	136901	1.090	1.240	-	-	230.0	7.200	0.391	1	H-lum	K2III	a
GX Lib	136905	-	-	-	-	-	-	-	1	MS	[G-KV]	
GX Lib	136905	0.730	1.020	0.840	0.550	-	7.290	0.6	1	H-lum	K1III	a,j
LS TrA	137164	0.780	1.040	0.836	0.554	54.0	8.063	4.401	2	T-RGB	K2IV	b,kc
LS TrA	137164	0.780	1.040	0.836	0.554	54.0	8.063	4.401	2	T-RGB	K2IV	b,kc
WW Dra	150708	0.040	0.600	-	-	180.0	-	2.304	2	MSoff	G2IV	d,m
WW Dra	150708	0.880	1.100	0.720	-	180.0	-	3.338	2	T-RGB	K0IV	a,m
epsilon UMi	153751	-	-	-	-	71.0	-	2.55	1	MS	A8-F0V	j
epsilon UMi	153751	0.550	0.890	-	0.470	71.0	4.230	0.080	1	H-lum	G5III	a,i
V792 Her	155638	-	0.450	-	-	310.0	-	2.349	2	MSoff	F2IV	m
V792 Her	155638	-	1.070	-	-	310.0	-	0.838	2	H-lum	K0III	d,m
HR 6469	157482	-	-	-	-	69.0	-	3.6	1	MS	{F2V}	j
HR 6469	157482	-	-	-	-	69.0	-	4.4	1	MS	{G0V}	j
HR 6469	157482	0.210	0.680	0.490	-	69.0	5.510	1.316	1	H-lum	G5IV	a
29 Dra	160538	-	-	-	-	87.9	-	-	1	WD	WD	
29 Dra	160538	0.810	1.050	-	-	87.9	6.550	1.830	1	T-RGB	K0-2III	a
HR 6626	161832	1.460	1.390	-	-	250.0	6.680	-0.310	1	H-lum	K3III	a
V832 Ara	165141	-	-	-	-	170.0	-	-	1	WD	WD	
V832 Ara	165141	0.610	1.010	0.766	0.493	170.0	7.080	0.928	1	H-lum	G8III	a,kc
omicron Dra	175306	1.040	1.190	-	0.640	67.0	4.640	0.510	1	H-lum	G9III	a
HR 7275	179094	0.870	1.090	0.810	-	250.0	5.810	-1.180	1	H-lum	K1IV-III	a
V4138 Sgr	181809	0.710	1.030	0.860	0.540	210.0	6.570	-0.041	1	H-lum	K1III	a
V4139 Sgr	182776	1.038	1.221	0.961	0.626	-	8.400	0.4	1	H-lum	K2-3III	a,kc,j
HR 7428	184398	-	-	-	-	302.0	-	1.3	2	MS	A2V	j
HR 7428	184398	0.910	1.160	-	-	302.0	6.320	-0.951	2	H-lum	K2III-II	a,i
V1764 Cyg	185151	-	-	-	-	390.0	-	-	2	MS	F	
V1764 Cyg	185151	-	1.250	1.050	0.670	390.0	7.690	-0.265	2	H-lum	K1III	a
V1379 Aql	185510	-	-	-	-	-	-	-	1	subMS	sdB	
V1379 Aql	185510	0.690	1.130	0.990	0.670	-	8.320	1.9	1	T-RGB	K0IV-III	a,j
V4091 Sgr	190540	1.020	1.200	0.980	0.610	-	8.380	0.7	1	H-lum	K0III	a,j
BN Mic	202134	0.887	1.086	0.877	0.575	-	7.720	0.6	1	H-lum	K1IIIp	a,kc,j
AS Cap	205249	0.770	0.900	0.766	0.503	93.0	7.680	2.838	1	B-RGB	K1III	a,kc
HK Lac	209813	-	-	-	-	150.0	-	3.15	1	MS	F1V	j
HK Lac	209813	0.760	1.080	0.750	0.585	150.0	6.520	0.735	1	H-lum	K0III	a,d,kc,i
V350 Lac	213389	1.000	1.170	0.840	-	69.0	6.380	2.186	1	T-RGB	K2III	a
IM Peg	216489	0.900	1.120	0.900	-	50.0	5.600	2.105	1	T-RGB	K2III-II	a
KU Peg	218153	-	1.120	-	-	-	7.900	-2.3	1	II	G8II	a,j
SZ Psc	219113	0.000	0.440	-	-	125.0	-	3.3	2	MS	F8IV	h
SZ Psc	219113	0.650	1.000	0.700	0.350	125.0	-	2.3	2	T-RGB	K1IV	a,d,h
lambda And	222107	0.690	1.010	0.780	0.570	23.0	3.700	1.891	1	T-RGB	G8IV-III	a
II Peg	224085	0.660	1.010	0.890	0.500	29.4	7.200	4.858	1	B-RGB	K2-3V-IV	a

a.- The color indices include the contribution of the secondary, except when the color for the secondary are given.

b.- Two equal stars: $(U-B)_p=(U-B)_s=(U-B)_{obs}$, $V_p=V_s=V_{obs}+0.753$.

c.- The hot component dominates (U-B)

d.- There are also available M_V^p , M_V^s .

e.- It is possible to deconvolve the photometry in V.

f.- Combined M_V .

g.- The hot component dominates (B-V).

h.- M_V (hot/cool) were calculated independently during the eclipses.

i.- M_V (primary) were calculated by a deconvolution with the M_V (total) and M_V (secondary):

$$V_p = V_s - 2.5 \text{ Log} [10^{-(V_{total}-V_s)/2.5} - 1]$$

j.- M_V assumed from the spectral type.

k.- From the Strassmeier et al. catalogue.

l.- Distance from M_V , V.

m.- M_V from R, T_{eff} , CB.

Table 2: Equivalent widths and correction factors

Name	HD	T_{eff} (K)	Radius (R_{\odot})	Equiv. width					CCF	Comments
				Li+Fe (Å)	Fe (Å)	(Li+Fe) P92 (Å)	Fe P92 (Å)	Li (Å)		
(1)	(2)	(3)	(4)	(5)	(6)	(7)	(8)	(9)	(10)	(11)
33 Psc	28	4651	-	38	18	38	(30)	17	-	
5 Cet	352	-	-	-	-	-	-	-	-	
5 Cet	352	3928	-	32	17	-	-	14.6	-	
BD Cet	1833	4460	-	-	-	30	(36)	-	-	
zeta And	4502	4481	-	73	20 ^c	-	-	53 ^c	-	
AY Cet	7672	-	-	-	-	-	-	-	-	
AY Cet	7672	4930	-	13	12	15	15	3.8	-	
UV For	10909	4725	-	-	-	14	14	-	-	
6 Tri	13480	6440	1.3	-	-	-	-	-	50.901	1
6 Tri	13480	5530	13	86	19	-	-	76	1.018	1
EL Eri	19754	4257	-	-	-	-	-	-	-	
BD+43 657	19942	5020	-	5	2.8	-	-	2.8	-	
HR 1023	21018	5154	-	222	23	-	-	205	-	
V711 Tau	22468	5460	1.3	-	-	-	-	-	8.626	1
V711 Tau	22468	5243	3.9	70	9 ^c	85	(26)	61 ^c	1.131	1
HR 1176	23838	6890	-	-	-	-	-	-	14.183	3
HR 1176	23838	6094	-	34	12	-	-	23	1.076	3
V492 Per	28591	4984	-	-	-	-	-	-	-	
3 Cam	29317	4643	-	31	28	-	-	4.5	-	
RZ Eri	30050	6645	2.83	-	-	-	-	-	2.329	1
RZ Eri	30050	4542	7.0	56	8 ^c	38	(28)	48 ^c	1.752	1
12 Cam	32357	4510	-	34	20 ^c	-	-	14 ^c	-	
CP-77 196	34802	4537	-	-	-	63	(36)	-	-	
alpha Aur	34029	5910	8.7	-	-	-	-	-	2.188	1
alpha Aur	34029	5124	12.6	-	-	-	-	-	1.842	1
TW Lep	37847	6357	-	-	-	-	-	-	8.413	3
TW Lep	37847	4433	-	-	-	70	(24)	-	1.135	3
V1149 Ori	37824	4457	-	85	29 ^c	91	(37)	56 ^c	-	
TY Pic	42504	-	-	-	-	-	-	-	-	
TY Pic	42504	4633	-	-	-	115	(24)	-	-	
TZ Pic	46697	4537	-	-	-	62	(36)	-	-	
AR Mon	57364	4900	10.8	-	-	-	-	-	2.223	1
AR Mon	57364	4545	14.2	-	-	100	(45)	-	1.817	1
V344 Pup	61245	4679	-	-	-	74	(37)	-	-	
sigma Gem	62044	4422	-	-	-	-	-	-	-	
LU Hya	71071	4946	-	-	-	46	26	-	-	
HR 3385	72688	5014	-	-	-	90	(35)	-	-	
RZ Cnc	73343	4600	10.2	-	-	-	-	-	2.111	1
RZ Cnc	73343	4365	12.2	-	-	-	-	-	1.901	1
IL Hya	81410	4650	-	-	-	113	(37)	-	-	
IN Vel	83442	4352	-	-	-	40	37	-	-	
DM UMa	-	4643	-	53	18 ^c	-	-	35 ^c	-	
CD-38 7259	101309	5770	-	-	-	-	-	-	2.785	3
CD-38 7259	101309	4648	-	-	-	86	(22)	-	1.569	3
HR 4492	101379	9520	-	-	-	-	-	-	3.314	3
HR 4492	101379	4808	-	-	-	50	(30)	-	1.432	3
93 Leo	102509	8035	1.7	-	-	-	-	-	4.641	1
93 Leo	102509	5621	5.9	35	18	-	-	19	1.275	1
HU Vir	106225	4435	-	-	-	-	-	-	-	
HR 4665	106677	4524	13	-	-	-	-	-	1.982	1
HR 4665	106677	4507	13	-	-	-	-	-	2.018	1
BD-04 3419	113816	4549	-	-	-	-	-	-	-	
RS CVn	114519	6700	1.99	35*	13	-	-	16.3	2.141	1
RS CVn	114519	4836	4.00	15	7	-	-	8.5	1.876	1
BM CVn	116204	4424	-	49	20	-	-	29	-	
HR 5110	118216	6938	3.10	26	2	-	-	6	1.179	1
HR 5110	118216	4660	2.85	"	5	-	-	7	6.565	1
V851 Cen	119285	4311	-	-	-	69	(42)	-	-	
V841 Cen	127535	4389	-	-	-	84	(26)	-	-	

Table 2: (continued)

Name	HD	T_{eff}	Radius	Equiv. width			CCF	Comments		
				Li+Fe	Fe	Li				
(1)	(2)	(K)	(R_{\odot})	(\AA)	(\AA)	(\AA)	(10)	(11)		
UV CrB	136901	4219	–	63	16	–	–	53	–	
GX Lib	136905	–	–	–	–	29	(36)	–	–	
GX Lib	136905	4601	–	29	24	–	–	5	–	
LS TrA	137164	4593	–	–	–	≤ 35	(27)	–	2.000	3
LS TrA	137164	4593	–	–	–	“	“	–	2.000	3
WW Dra	150708	5910	2.12	87*	4	–	–	34	2.158	1
WW Dra	150708	4580	3.9	21	13	–	–	7	1.863	1
epsilon UMi	153751	7370	1.7	–	–	–	–	–	13.131	1
epsilon UMi	153751	5011	12	54	23	–	–	32	1.082	1
V792 Her	155638	6539	2.58	54*	1	–	–	12	6.765	1
V792 Her	155638	4643	12.28	92*	11	–	–	71	1.174	1
HR 6469	157482	6890	1	–	–	–	–	–	(48.731)	1
HR 6469	157482	6030	–	–	–	–	–	–	–	
HR 6469	157482	5602	10	33	12	–	–	21	(1.021)	1
29 Dra	160538	–	–	–	–	–	–	–	–	
29 Dra	160538	4602	–	39	19 ^c	–	–	10 ^c	–	
HR 6626	161832	3914	–	30	10	–	–	20	–	
V832 Ara	165141	–	–	–	–	–	–	–	–	
V832 Ara	165141	4862	–	–	–	40	(24)	–	–	
omicron Dra	175306	4291	–	33	24	–	–	9	–	
HR 7275	179094	4569	–	–	–	–	–	–	–	
V4138 Sgr	181809	4613	–	–	–	53	(36)	–	1.666	3
V4139 Sgr	182776	4277	–	–	–	80	(36)	–	2.501	3
HR 7428	184398	8970	–	–	–	–	–	–	8.951	3
HR 7428	184398	4426	–	69	33	–	–	46	1.126	3
V1764 Cyg	185151	–	–	–	–	–	–	–	–	
V1764 Cyg	185151	4495	–	70	24 ^c	–	–	46 ^c	–	
V1379 Aql	185510	–	–	–	–	–	–	–	–	
V1379 Aql	185510	4140	–	–	–	55	(28)	–	–	
V4091 Sgr	190540	4302	–	–	–	59	(37)	–	–	
BN Mic	202134	4492	–	–	–	63	44	–	–	
AS Cap	205249	4809	–	–	–	120	(36)	–	–	
HK Lac	209813	7039	–	–	–	–	–	–	10.247	3
HK Lac	209813	4588	–	126	21 ^c	–	–	105 ^c	1.108	3
V350 Lac	213389	4393	–	54	9 ^c	–	–	45 ^c	–	
IM Peg	216489	4534	–	89	19 ^c	–	–	70 ^c	–	
KU Peg	218153	4534	–	33	18	–	–	16	–	
SZ Psc	219113	6500	1.50	–	–	–	–	–	7.235	1
SZ Psc	219113	5500	5.1	–	–	–	–	–	1.160	1
lambda And	222107	4599	–	27	17 ^c	–	–	10 ^c	–	
II Peg	224085	4702	–	53	18 ^c	–	–	35 ^c	–	

* Lines blended with other.

^c The contribution of the FeI 6707.4 \AA was estimated from the colors and the EW's of other iron lines.^{P92} From Pallavicini et al. (1992).

() Iron eq. width assumed by Pallavicini et al. (1992).

1.- CCF from temperatures and radii.

2.- CCF from magnitudes of cool and hot components of eclipsing binaries.

3.- CCF from total magnitude and magnitude of secondary component. Then, deconvolution in order to compute the magnitude of the primary component:

$$V_p = V_s - 2.5 \text{Log}[10^{-(V_{\text{total}} - V_s)/2.5} - 1]$$

Table 3: Final abundances and other stellar parameters

Name	HD	T_{eff}	EW(corr)	log N(Li)			Mass	P(orb)	P(phot)	log Age	
				Final	P92	R93					R94
(1)	(2)	(K)	(Å)	(5)	(6)	(7)	(8)	(M_{\odot})	(days)	(days)	(yr)
33 Psc	28	4651	17	0.41	≤ 0.1	≤ 0	-	$\sim 3.0^{RT}$	72.93	-	8.555^M
5 Cet	352	3928	14.6	-0.54	-	-	-	0.81	96.439	-	-
BD Cet	1833	4460	6.53^{R93}	-0.29	≤ -0.5	-0.25	-	-	35.100	34.46	-
zeta And	4502	4481	53	0.81	-	-	0.9	2.70	17.7692	$\sim P_{orb}$	8.659
AY Cet	7672	4930	3.8	0.12	≤ -0.5	≤ 0	-	2.09	56.824	77.22	9.017
UV For	10909	4725	-	-0.25^{R93}	≤ -0.25	-0.25	-	$\sim 1.3^{CM}$	15.05	32.28	9.630^M
6 Tri	13480	5530	77.52	2.39	-	-	-	$2.56^{M \sin^3 i}$	14.7339	$\sim P_{orb}$	8.736^M
EL Eri	19754	4257	31.78^{R93}	0.22	0.7	0.6	-	$\sim 1.7^{CM}$	48.263	47.96	9.164^M
BD+43 657	19942	5020	2.8	0.08	-	-	-	1.6^{CM}	45.779	22.0	9.337^M
HR 1023	21018	5154	205	3.35	-	-	-	2.75	287.201	-	8.655^M
V711 Tau	22468	5460	7.88^{R94}	1.01	-	≤ 1.0	1	1.1	2.83774	2.841	9.842
V711 Tau	22468	5243	68.99	1.90	1.4	1.2	1.3	1.4	2.83774	2.841	9.580
HR 1176	23838	6094	24.75	2.11	-	-	-	$\sim 5^{CM}$	962.8	-	7.972^M
V492 Per	28591	4984	43.05^{R94}	1.38	-	-	1.4	1.6^{CM}	21.2902	21.3	9.273^M
3 Cam	29317	4643	4.5	-0.19	-	-	-	$\sim 5^{CM}$	121	-	7.972^M
RZ Eri	30050	4542	84.1	1.20	1.19	1.35	-	1.62	39.2826	31.4	9.344
12 Cam	32357	4510	14	0.13	-	-	0.3	$\sim 5^{CM}$	80.895	85	7.972^M
CP-77 196	34802	4537	42.83^{R93}	0.75	0.55	0.85	-	$\sim 0.9^{CM}$	19.310	20.38	-
alpha Aur	34029	5910	145.59^{R94}	3.31	-	-	3.1	2.49	104.0214	8	8.731
alpha Aur	34029	5124	12.03^{R94}	0.85	-	-	0.6	2.56	104.0214	80	8.667
TW Lep	37847	4433	46.45^{R94}	0.66	1.08	1.05	1.1	$\sim 5^{CM}$	28.344	28.22	7.972^M
V1149 Ori	37824	4457	56	0.80	0.8	0.7	-	4.5^{CM}	53.580	54.1	8.092^M
TY Pic	42504	4633	72.21^{R93}	1.23	1.5	1.4	-	1.7^{CM}	106.74	43.76	9.204^M
TZ Pic	46697	4537	-	0^{R93}	0.4	0	-	-	13.637	13.07	-
AR Mon	57364	4900	-	-0.1^{R94}	-	-0.1	-0.1	2.7	21.20812	$\sim P_{orb}$	8.696
AR Mon	57364	4545	-	1.2^{R94}	1.5	1.3	1.2	0.8	21.20812	$\sim P_{orb}$	"
V344 Pup	61245	4679	29.8^{R93}	0.74	0.87	0.8	-	$\sim 5^{CM}$	11.761	11.47	7.972^M
sigma Gem	62044	4422	52.85^{R94}	0.73	-	-	0.9	$\sim 5^{CM}$	19.60447	19.410	7.972^M
LU Hya	71071	4946	19.67^{R93}	0.88	0.97	0.95	-	1.3^{CM}	16.537	21.	9.630^M
HR 3385	72688	5014	37.8^{R93}	1.34	1.38	1.2	-	$\sim 5^{CM}$	45.130	19.34	7.972^M
RZ Cnc	73343	4600	84.6^{R94}	1.29	-	-	1.3	3.2	21.64303	$\sim P_{orb}$	8.500
RZ Cnc	73343	4365	-	0.5^{R94}	-	-	0.5	0.54	21.64303	$\sim P_{orb}$	"
IL Hya	81410	4650	73.1^{R93}	1.26	1.34	1.35	-	$\sim 5^{CM}$	12.908	12.89	7.972^M
IN Vel	83442	4352	-	$\leq 0.4^{R93}$	≤ -0.5	≤ -0.4	-	4.5^{CM}	52.270	54.95	8.092^M
DM UMa	-	4643	35	0.78	-	-	-	-	7.4949	7.478	-
CD-38 7259	101309	4648	74.2^{R93}	1.27	1.6	1.45	-	0.29	11.710	11.66	-
HR 4492	101379	4808	33.87^{R93}	0.99	0.68	1.0	-	2.5	61.360	56.03	8.763^M
93 Leo	102509	5621	24.23	1.69	-	-	-	$2.08^{M \sin^3 i}$	71.6900	55	8.973^M
HU Vir	106225	4435	$\leq 15^{R94}$	≤ 0.6	-	-	≤ 0.5	2.5^{CM}	10.3876	10.28	8.707^M
HR 4665	106677	4524	26.04^{R94}	0.44	-	-	0.5	$1.92^{M \sin^3 i}$	64.44	63.75	9.065^M
HR 4665	106677	4507	31.78^{R94}	0.54	-	-	0.6	$1.92^{M \sin^3 i}$	64.44	63.75	9.065^M
BD-04 3419	113816	4549	-	0.8^{R94}	-	-	0.8	1.2^{CM}	$\sim 20.$	-	9.602^M
RS CVn	114519	4836	15.95	0.63	-	-	0.91	1.44	4.797851	4.7912	9.446
BM CVn	116204	4424	29	0.38	-	-	0.3	$\sim 5^{CM}$	20.625	20.6	7.972^M
HR 5110	118216	6938	7.07	~ 3.01	-	-	-	1.5	2.613214	$\sim P_{orb}$	9.272
HR 5110	118216	4660	45.96	0.96	-	-	1.5	0.8	2.613214	$\sim P_{orb}$	"
V851 Cen	119285	4311	44.67^{R93}	0.47	0.62	0.95	-	$\sim 0.9^{CM}$	11.989	12.05	-
V841 Cen	127535	4389	60.81^{R93}	0.77	1.15	1.15	-	-	5.998	5.929	-

Table 3: (continued)

Name	HD	T_{eff}	EW(corr)	log N(Li)				Mass	P(orb)	P(phot)	log Age
				Final	P92	R93	R94				
(1)	(2)	(K)	(Å)	(5)	(6)	(7)	(8)	(M_{\odot})	(days)	(days)	(yr)
UV CrB	136901	4219	53	0.46	–	–	0.1	1.06	18.6651	$\sim P_{orb}$	9.743 ^M
GX Lib	136905	4601	5	-0.20	≤ -0.45	-0.3	–	$\sim 5^{CM}$	11.1345	11.134	7.972 ^M
LS TrA	137164	4593	17.08 ^{R93}	0.33	≤ 1.03	0.5	–	–	49.431	49.19	–
LS TrA	137164	4593	17.08 ^{R93}	0.33	“	0.5	–	–	49.431	49.19	–
WW Dra	150708	4580	13.04	0.19	–	–	–	1.34	4.629617	$\sim P_{orb}$	9.646
epsilon UMi	153751	5011	34.62	1.28	–	–	–	2.8	39.4809	$\sim P_{orb}$	8.652
V792 Her	155638	4643	83.35	1.34	–	–	–	1.47	27.5368	27.07	9.466
HR 6469	157482	5602	21.44	1.66	–	–	1.6	2.05	2018	81.09	8.939
29 Dra	160538	4602	10	0.10	–	–	≤ 0	2.5 ^{CM}	905.9	31.5	8.736 ^M
HR 6626	161832	3914	20	-0.42	–	–	–	$\sim 5^{CM}$	99.559	$\sim P_{orb}$	7.972 ^M
V832 Ara	165141	4862	5.74 ^{R93}	0.20	0.45	0.05	–	4.5 ^{CM}	5200	34.60	8.092 ^M
omicron Dra	175306	4291	9	-0.34	–	–	≤ 0	5 ^{CM}	138.420	142.8	7.972 ^M
HR 7275	179094	4569	31.78 ^{R94}	0.63	–	–	0.6	$\geq 5^{CM}$	28.5895	$\sim P_{orb}$	7.972 ^M
V4138 Sgr	181809	4613	42.67 ^{R93}	0.86	0.47	1.0	–	$\geq 5^{CM}$	13.048	60.23	7.972 ^M
V4139 Sgr	182776	4277	–	0.93	0.35	0.	–	4.5 ^{CM}	45.180	45.180	8.092 ^M
HR 7428	184398	4426	40.54	0.58	–	–	0.2	4.83	108.854	$\sim P_{orb}$	8.029
V1764 Cyg	185151	4495	46	0.73	–	–	0.8	1.5	40.1418	39.878	9.296
V1379 Aql	185510	4140	32.93 ^{R93}	0.09	0.38	0.55	–	1.7 ^{CM}	20.660	25.64	9.204 ^M
V4091 Sgr	190540	4302	–	0.1 ^{R93}	0.04	0.1	–	3.7 ^{CM}	16.887	16.6	8.318 ^M
BN Mic	202134	4492	6.52 ^{R93}	-0.25	0.4	-0.1	–	5 ^{CM}	63.09	61.73	7.972 ^M
AS Cap	205249	4809	66.65 ^{R93}	1.43	1.8	1.8	1.7	2.0 ^{CM}	49.137	57.90	9.018 ^M
HK Lac	209813	4588	70.06 ^{R94}	1.15	–	–	1.40	$\sim 5^{CM}$	24.4284	24.461	7.972 ^M
V350 Lac	213389	4393	45	0.58	–	–	0.2	1.1	17.755	$\sim P_{orb}$	9.701 ^M
IM Peg	216489	4534	70	1.07	–	–	–	1.5 ^{CM}	24.65	24.39	9.347 ^M
KU Peg	218153	4534	16	0.22	–	–	–	$\geq 5^{CM}$	1411	22	7.972 ^M
SZ Psc	219113	5500	44.32 ^{R94}	1.96	–	–	1.6	1.62	3.965866	3.955	9.350
lambda And	222107	4599	10	0.09	–	–	≤ -0.5	2.5 ^{CM}	20.5212	53.952	8.763 ^M
II Peg	224085	4702	35	0.86	–	–	1.1	–	6.724183	6.718	–

P92.- Abundance from Pallavicini et al. (1992).

R93, R94.- EW(Li) and abundances after Randich et al. (1993; 1994).

CM.- Mass estimated from the Color–Magnitude Diagram.

Msin³i.- Mass computed from the $M \times \sin^3 i$.

RT.- Mass estimated from the Radius– T_{eff} plane.

P_{orb} .- Photometric period similar to the orbital period.

M.- Age estimated from the Age–Mass relation.